

## Atomistic-to-continuum description of edge dislocation core: Unification of the Peierls-Nabarro model with linear elasticity

Max Boleininger,<sup>1,\*</sup> Thomas D. Swinburne,<sup>2,†</sup> and Sergei L. Dudarev<sup>1,‡</sup>

<sup>1</sup>*CCFE, Culham Science Centre, UK Atomic Energy Authority, Abingdon, Oxfordshire OX14 3DB, United Kingdom*

<sup>2</sup>*Theoretical Division T-1, Los Alamos National Laboratory, Los Alamos, New Mexico 87545, USA*



(Received 15 April 2018; published 31 August 2018)

Conventional linear elasticity theory predicts the strain fields of a dislocation core to diverge, whereas it is known from atomistic simulations that core strains should remain finite. We present an analytical solution to a generalized, variational Peierls-Nabarro model of edge dislocation displacement fields that features a finite core width and correct isotropic elastic behavior at large distances away from the core. We derive an analytical expression for the dislocation core radius, representing the convergence radius of the linear elasticity far-field expansion. The strain fields are in qualitative agreement with atomistic simulations of  $\frac{1}{2}[111](10\bar{1})$  edge dislocations in bcc tungsten and iron. The treatment is based on the multistring Frenkel-Kontorova model that we reformulate as a generalized Peierls-Nabarro model using the principle of least action.

DOI: [10.1103/PhysRevMaterials.2.083803](https://doi.org/10.1103/PhysRevMaterials.2.083803)

### I. INTRODUCTION

The assessment of accuracy of the line-tension model for modeling dislocations is essential for deriving physical models for dislocation energetics in dislocation dynamics simulations. Linear elasticity predicts that straight dislocations have negative line tension with respect to small fluctuations [1,2], suggesting that the energy of a dislocation would decrease as a result of it bowing out. This is in stark contrast to atomistic simulations that consistently predict positive line tension. The central problem of linear elasticity theory in this context is its inability to describe the displacement field of the dislocation core: The strain field of the dislocation is found to diverge in the glide plane, leading to infinite energy density unless the divergence is cut out or otherwise regularized. A physically consistent treatment of the dislocation core is therefore a prerequisite for correctly describing dislocation line tension in a continuum model.

It was shown by Peierls [3] that the divergence can be resolved by the inclusion of a periodic misfit potential, representing the forces of the periodic arrangement of atoms in the crystal lattice. The misfit potential energetically penalizes concentrations of strain, causing the dislocation core to spread out and attain a finite size. Models developed later [4–6] offer a connection between the generalized stacking fault energy and various phenomena involving dislocation cores. Yet a common drawback of these models is either an incomplete description of elasticity away from the core, or the lack of tractable analytical solutions.

We present a continuum theory of edge dislocation that features a finite core size, as in the Peierls-Nabarro [7] model,

as well as a displacement field which is consistent with linear isotropic elasticity theory away from the core. The displacement fields are found to be in agreement with the atomistic displacements derived from molecular dynamics simulations of body-centered-cubic (bcc) iron and tungsten, provided that the dislocation core is wide enough to agree with the underlying continuum approximation. The model is derived from the discrete multistring Frenkel-Kontorova [8] (MSFK) model, which in the continuum limit unifies linear elasticity and the Peierls-Nabarro model in a consistent manner.

The derivation of the continuum equations from the MSFK model is outlined in Sec. II. The continuum model compatible with both the Peierls-Nabarro model and isotropic linear elasticity theory is presented and solved analytically in Sec. III for a straight edge dislocation.

### II. ANALYTICAL SOLUTION FOR THE STRAIN FIELD OF A STRAIGHT EDGE DISLOCATION

Atoms in the multistring Frenkel-Kontorova model are considered to interact harmonically with their nearest neighbors in the direction parallel to the Burgers vector, forming linear elastic strings. Each atom also feels the effect of sinusoidal potentials from the neighboring strings, which may be locally shifted with respect to a reference string. To make an analytical solution possible, atoms are constrained to only move along the direction of the Burgers vector. Consequently the model only delivers the displacement field parallel to the Burgers vector of the dislocation.

Let the atomic positions  $x_{n,j}$  be indexed by their position  $n$  within a string and by the vector-valued index  $j$  representing the string location in a plane orthogonal to the Burgers vector, as illustrated in Fig. 1. As the strings are parallel to the Burgers vector, in a monoatomic lattice the equilibrium atomic spacing along the string is the Burgers vector length  $b$ . The discrete Lagrangian is expressed in terms of atomic displacements

\*max.boleininger@ukaea.uk

†tomswinburne@gmail.com

‡sergei.dudarev@ukaea.uk

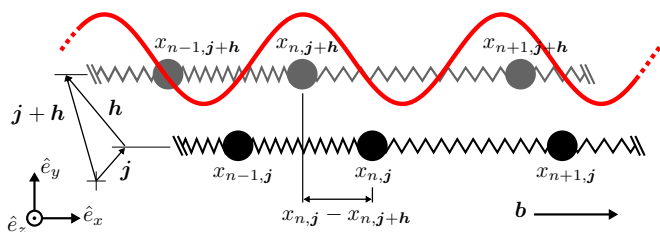


FIG. 1. The multistring Frenkel-Kontorova model pictured in the  $xy$  plane. Atoms in the lattice are classified by dividing the lattice into atomic strings lying parallel to the Burgers vector  $\mathbf{b}$ . Neighboring atoms in a string interact harmonically. Each atom  $x_{n,j}$  interacts with the surrounding strings via a sinusoidal potential shifted by the displacement of a reference atom  $x_{n,j+h}$ .

$$u_{n,j} = x_{n,j} - nb \text{ as}$$

$$\mathcal{L} = \sum_j \sum_{n=-\infty}^{\infty} \left( \frac{m\dot{u}_{n,j}^2}{2} - \frac{\alpha}{2} (u_{n+1,j} - u_{n,j})^2 \right) - \frac{m\omega^2 b^2}{2\pi^2} \sum_{j,h} \sum_{n=-\infty}^{\infty} \sin^2 \left( \frac{\pi}{b} (u_{n,j} - u_{n,j+h}) \right), \quad (1)$$

where  $m$  is the atomic mass. For the edge dislocation geometry considered here, the natural frequency  $\omega$  characterizes the strength of interaction between the strings, and  $\alpha$  characterizes the stiffness of harmonic interaction between neighboring atoms in a string. Vector summation runs over the string positions  $\mathbf{j}$  and the displacement vector  $\mathbf{h}$  of their respective nearest neighbors.

We shall next introduce a dislocation into the material. For this purpose we divide  $\mathbb{R}^3$  into two volumes,  $\Omega^+$  and  $\Omega^-$ , separated by the dividing surface,  $\partial\Omega$ , as illustrated in Fig. 2. Note that the dividing surface must not cut atomic strings; the surface normal is perpendicular to the string direction at any point in space, hence  $n_x = 0$ . The edge dislocation is introduced as a discontinuity in the displacement boundary

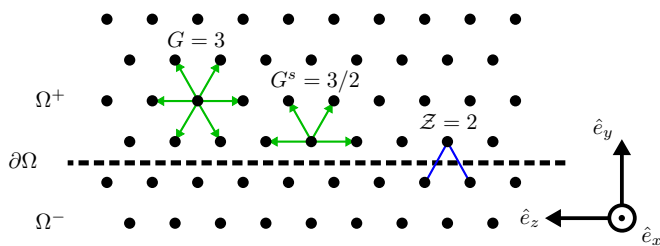


FIG. 2. Continuum representation of the string summation terms for the example of a bcc  $\frac{1}{2}[111](10\bar{1})$  edge dislocation, where  $\mathbf{b} \parallel \hat{e}_x$ . The black dots represent MSFK strings as seen in the direction parallel to the Burgers vector. Vectors shown in green illustrate summation over string-neighbor vectors  $\mathbf{h}$ . Note that summation is not performed across the glide plane  $\partial\Omega$  (dashed line), leading to the structure constant  $G$  to adopt different values at the surface and in the bulk. The effective number of strings interacting across the plane in this example is  $\mathcal{Z} = 2$ .

conditions as the dividing surface is crossed:

$$\lim_{n \rightarrow -\infty} u_{n,j} = b/2 \quad \text{and} \quad \lim_{n \rightarrow \infty} u_{n,j} = 0, \quad \mathbf{j} \in \Omega^+, \\ \lim_{n \rightarrow -\infty} u_{n,j} = -b/2 \quad \text{and} \quad \lim_{n \rightarrow \infty} u_{n,j} = 0, \quad \mathbf{j} \in \Omega^-. \quad (2)$$

The dividing surface  $\partial\Omega$  is therefore equivalent to the dislocation glide plane.

The Lagrangian (1) only depends on the difference between atomic displacements that are generally considered to vary slowly in space. An exception occurs when two neighboring strings lie on opposite sides of the dividing surface due to the discontinuity introduced through the boundary conditions. The displacement field difference between strings within the same domain  $\Omega^+$  or  $\Omega^-$  however is considered small, and the potential can therefore be linearized. The Lagrangian is split into three parts: two for the  $\Omega^+$  and  $\Omega^-$  domains and one for the dividing surface  $\partial\Omega$ , namely

$$\mathcal{L} = \mathcal{L}_{\Omega^+} + \mathcal{L}_{\Omega^-} + \mathcal{L}_{\partial\Omega}, \quad (3)$$

where:

$$\mathcal{L}_{\Omega^\pm} = \sum_{j \in \Omega^\pm} \sum_{n=-\infty}^{\infty} \left( \frac{m\dot{u}_{n,j}^2}{2} - \frac{\alpha}{2} \left( \frac{\partial u_{n,j}}{\partial n} \right)^2 \right) - \frac{m\omega^2}{2} \sum_{j \in \Omega^\pm} \sum_{n=-\infty}^{\infty} \sum_{j+h \in \Omega^\pm} \left( \frac{\partial u_{n,j}}{\partial \mathbf{h}} \right)^2 \quad (4a)$$

$$\mathcal{L}_{\partial\Omega} = -\frac{m\omega^2 b^2}{\pi^2} \sum_{j \in \Omega^+} \sum_{n=-\infty}^{\infty} \sum_{j+h \in \Omega^-} \sin^2 \left( \frac{\pi}{a} (u_{n,j} - u_{n,j+h}) \right). \quad (4b)$$

The summation in the surface term  $\mathcal{L}_{\partial\Omega}$  runs over all the neighboring string pairs on the opposing sides of the dividing surface. The factor of 2 compared to the original Lagrangian (1) is accounting for double counting in the string summation.

In the continuum limit, the atomic displacements defined in  $\Omega^\pm$ , respectively, become continuous scalar fields  $u^\pm = u^\pm(\mathbf{r}, t)$ . The Lagrangian of the discrete system hence becomes a volume integral over the Lagrange density:

$$L = L_{\Omega^+} + L_{\Omega^-} + L_{\partial\Omega} \\ L_{\Omega^\pm} = \eta \int_{\Omega^\pm} dV \left( \frac{m(\dot{u}^\pm)^2}{2} - \frac{\alpha b^2}{2} \left( \frac{\partial u^\pm}{\partial x} \right)^2 - \frac{m\omega^2 l^2}{2} \sum_h \left( \hat{e}_h^y \frac{\partial u^\pm}{\partial y} + \hat{e}_h^z \frac{\partial u^\pm}{\partial z} \right)^2 \right) \\ L_{\partial\Omega} = \int_{\partial\Omega} dS \left( -\mathcal{Z} \frac{m\omega^2 b^2}{\pi^2 l} \right) \sin^2 \left( \frac{\pi}{b} (u^+ - u^-) \right), \quad (5)$$

where  $\eta$  is the atom number density,  $l$  is the perpendicular distance between neighboring strings,  $\hat{e}_h^y = \hat{e}_y \cdot \mathbf{h} / \|\mathbf{h}\|$ , and  $\mathcal{Z}$  refers to the effective number of neighboring strings that lie across the dividing surface. The displacement fields on the dividing surface are defined in terms of the limit approaching

the surface, namely

$$u^\pm(\mathbf{r}) = \lim_{\gamma \rightarrow 0} u^\pm(\mathbf{r} - \gamma \mathbf{n}^\pm(\mathbf{r})), \quad \mathbf{r} \in \partial\Omega, \quad (6)$$

where  $\mathbf{n}^\pm(\mathbf{r})$  are the outwards-facing surface normals of the domains  $\Omega^\pm$ , hence  $\mathbf{n}^+(\mathbf{r}) = -\mathbf{n}^-(\mathbf{r})$ .

Some subtleties are involved in taking the continuum limit. Consider the second term in Eq. (4a). The string summation is performed in such a way that only strings within the same domain  $\Omega^+$  or  $\Omega^-$  interact; the interaction does not cross the glide plane  $\partial\Omega$ , as the nonlinear interaction of strings across  $\Omega^+$  and  $\Omega^-$  is already captured in Eq. (4b). Summation over the neighboring strings  $\mathbf{h}$  in Eq. (5) therefore leaves out the strings lying across the glide plane  $\partial\Omega$  if integration is performed over the surface, which is indicated by the primed summation symbol. We refer to Fig. 2 for a visual guide.

We proceed by minimizing the action associated with the Lagrangian with respect to variation in displacement fields and their derivatives. Let the action be defined as the time integral over the Lagrangian:

$$S[u] = \int dt L[u, u_i], \quad (7)$$

where the coordinate  $i$  refers both to spatial and time coordinates, and  $u_i = \partial_i u(\mathbf{r}, t)$ . The stationary point of the action  $\delta S[u] = 0$  is found by variation of the scalar field and its first order derivatives:

$$\delta S[u] = \int dt \left( \frac{\partial L[u, u_i]}{\partial u} \delta u + \frac{\partial L[u, u_i]}{\partial u_i} \delta u_i \right) \stackrel{!}{=} 0. \quad (8)$$

The derivatives  $\partial/\partial u$  and  $\partial/\partial u_i$  are understood as functional derivatives. Note that we consider the variation  $\delta u$  not to vanish at the  $\partial\Omega$  boundary, as we are looking to find the displacement field at the glide plane. Applying integration by parts and the divergence theorem yields the MSFK equations of motion from the stationary condition:

$$\begin{aligned} 0 &= -\ddot{u}^+ + c^2 u_{xx}^+ + \omega^2 l^2 G (u_{yy}^+ + u_{zz}^+), \quad \mathbf{r} \in \Omega^+ \\ 0 &= -\ddot{u}^- + c^2 u_{xx}^- + \omega^2 l^2 G (u_{yy}^- + u_{zz}^-), \quad \mathbf{r} \in \Omega^- \\ 0 &= G_{yy}^s u_y^+ n_y^+ + G_{zz}^s u_z^+ n_z^+ + 2G_{yz}^s (n_y^+ u_z^+ + n_z^+ u_y^+) \\ &\quad + \frac{\mathcal{Z}}{\pi \eta l^3} \sin\left(\frac{2\pi}{b}(u^+ - u^-)\right), \quad \mathbf{r} \in \partial\Omega \\ 0 &= G_{yy}^s u_y^- n_y^- + G_{zz}^s u_z^- n_z^- + 2G_{yz}^s (n_y^- u_z^- + n_z^- u_y^-) \\ &\quad - \frac{\mathcal{Z}}{\pi \eta l^3} \sin\left(\frac{2\pi}{b}(u^+ - u^-)\right), \quad \mathbf{r} \in \partial\Omega, \quad (9) \end{aligned}$$

where  $\alpha b^2/m = c^2$ , and  $u_i = \partial u/\partial i$ . The structure constant  $G_{ij}$  is defined as  $G_{ij} = \sum_{\mathbf{h}} \hat{e}_i^{\mathbf{h}} \hat{e}_j^{\mathbf{h}}$ , and equals  $G_{ij} = G \delta_{ij}$  in the bulk, where  $G = 2$  for the square lattice and  $G = 3$  for the hexagonal lattice. The value of constant  $G_{ij}^s$  in the glide plane depends on the geometry of the dislocation cut, as lattice vectors  $\mathbf{h}$  crossing the glide plane are left out of the summation. Note that we have used condition  $n_x^\pm = 0$ .

We shall next restrict ourselves to the treatment of a straight edge dislocation, by aligning the dividing surface with the  $xz$  plane. Domains  $\Omega^\pm$  now become the upper and lower open

half planes in  $\mathbb{R}^2$ , respectively,

$$\begin{aligned} \Omega^+ &= \{(x, y) \in \mathbb{R}^2 \mid y > 0\} \\ \Omega^- &= \{(x, y) \in \mathbb{R}^2 \mid y < 0\} \\ \partial\Omega &= \{(x, y) \in \mathbb{R}^2 \mid y = 0\}, \end{aligned} \quad (10)$$

with the normal vector components of  $n_y^\pm = \mp 1$  and  $n_z^\pm = 0$ . The  $z$  coordinate can be left out as the edge dislocation strain fields are translationally invariant along the line direction  $\hat{e}_z$ , hence  $u_z^\pm = u_{zz}^\pm = 0$ . We further consider the dislocation to be static,  $\ddot{u}^\pm = 0$ , to arrive at the elastostatic equations. Equations of motion now reduce to a boundary value problem:

$$u_{xx}^+ + \frac{\omega^2 l^2 G}{c^2} u_{yy}^+ = 0, \quad y > 0 \quad (11a)$$

$$u_{xx}^- + \frac{\omega^2 l^2 G}{c^2} u_{yy}^- = 0, \quad y < 0 \quad (11b)$$

$$\begin{aligned} \frac{\pi \eta l^3 G^s}{\mathcal{Z}} u_y^+ &= \frac{\pi \eta l^3 G^s}{\mathcal{Z}} u_y^- \\ &= \sin\left(\frac{2\pi}{b}(u^+ - u^-)\right), \quad y = 0, \quad (11c) \end{aligned}$$

where  $G^s = G_{yy}^s$ . This boundary value problem is reminiscent of Peierls' formalism [3], although the MSFK equations of motion have a more general range of validity and span the entire space  $\mathbb{R}^2$ .

At this point we can also establish a connection between the nonsingular MSFK model and the isotropic elastostatic equations. The elastostatic equations follow from Hooke's law,  $\sigma_{ij} = \sum_{kl} c_{ijkl}(u_{k,l} + u_{l,k})/2$ , the stationary stress condition,  $\sum_j \sigma_{ij,j} = 0$ , and plane-strain conditions,  $u_z = 0$ :

$$\begin{aligned} u_{x,xx} + \frac{1-2\nu}{2(1-\nu)} u_{x,yy} &= -\frac{1}{2(1-\nu)} u_{y,xy} \\ u_{y,yy} + \frac{1-2\nu}{2(1-\nu)} u_{y,xx} &= -\frac{1}{2(1-\nu)} u_{x,yx}. \end{aligned} \quad (12)$$

The elastostatic equations can be matched to MSFK by restricting the displacements to only occur in the  $u_x$  direction:

$$u_{x,xx} + \frac{1-2\nu}{2(1-\nu)} u_{x,yy} = 0. \quad (13)$$

From this comparison we identify the MSFK constant  $\frac{\omega^2 l^2 G}{c^2}$  as  $\frac{1-2\nu}{2(1-\nu)}$ , leading to the MSFK definition of Poisson's ratio:

$$\nu = \frac{\alpha b^2 - 2Gl^2 m \omega^2}{2(\alpha b^2 - Gl^2 m \omega^2)}. \quad (14)$$

We note that (14) shows that the ratio of deformations along  $x$  and  $y$  can be simply written in terms of the energy stored in springs of strength  $\alpha$  and  $m\omega^2$  extended to respective interatomic spacings  $b$  and  $l$ .

We now need to solve the problem posed by Eqs. (11a)–(11c). Consider the function  $w(x, y) = u^-(x, -y)$ , which has the same support as  $u^+$ . It is simple to show that the sum  $w(x, y) + u^+(x, y)$  obeys the Laplace equation in  $y > 0$ , is identically zero in the limit  $x \rightarrow \pm\infty$  for  $y > 0$  and satisfies  $d/dy(w + u^+) = 0$  on  $y = 0$ . By the uniqueness of solutions to the Laplace equation, we find by inspection that  $(w +$

$u^+$ ) = 0 everywhere on  $y \geq 0$ , giving the symmetry relation  $u^+(x, y) = -u^-(x, -y)$ . Using this relation, which we note is obeyed by the Volterra solution for an edge dislocation, we only need to consider the following boundary value problem in the upper half plane:

$$\begin{aligned} u_{xx}^+ + \frac{1-2\nu}{2(1-\nu)} u_{yy}^+ &= 0, \quad y > 0 \\ \frac{4\pi}{p} u_y^+ &= \sin\left(\frac{4\pi}{b} u^+\right), \quad y = 0, \end{aligned} \quad (15)$$

where  $p = \mathcal{Z}/(\eta l^3 G^s)$  is the dimensionless surface structure constant. The solution to the problem above, after some minor substitutions, has been found by Dudarev [8], namely

$$\begin{aligned} u^+(x, y) &= \frac{b}{2\pi} \left( \frac{\pi}{2} - \arctan\left(\frac{px}{b+py} \sqrt{\frac{1-2\nu}{2(1-\nu)}}\right) \right), \quad y > 0 \\ u^-(x, y) &= \frac{b}{2\pi} \left( -\frac{\pi}{2} + \arctan\left(\frac{px}{b-py} \sqrt{\frac{1-2\nu}{2(1-\nu)}}\right) \right), \quad y < 0, \end{aligned} \quad (16)$$

or

$$u(x, y) = \frac{b}{2\pi} \operatorname{sgn}(y) \left( \frac{\pi}{2} - \arctan\left(\frac{px}{b+p|y|} \sqrt{\frac{1-2\nu}{2(1-\nu)}}\right) \right), \quad y \in \mathbb{R} \setminus \{0\}, \quad (17)$$

where  $\operatorname{sgn}$  is the sign function:  $\operatorname{sgn}(x) = 1$  if  $x \geq 0$ , otherwise  $-1$ .

A useful measure for the dislocation core width  $w$  is the full width at half maximum of the  $\partial u(x, y)/\partial x$  strain field in the glide plane, that is for  $y \rightarrow 0$ :

$$w = \frac{2b}{p} \sqrt{\frac{2(1-\nu)}{1-2\nu}}. \quad (18)$$

The key feature of this solution is that the core width  $w$  remains finite as predicted by atomistic simulations; the strain field  $\partial u(x, y)/\partial x$  does not diverge at the glide plane. Another interesting finding is that the dimensionless surface-structure constant  $p = \mathcal{Z}/(\eta l^3 G^s)$  controlling the core width is solely determined by the crystal structure and the geometry of the edge dislocation cut. This suggests that the width of the dislocation core does not depend on the details of the chosen interatomic potential. We have so far neglected the displacement field perpendicular to the Burgers vector. This is evident in the simplification of the elastostatic Eqs. (12) to (13).

Concluding this section we summarize and elaborate the approximations taken up to this point:

(i) The discrete MSFK Lagrangian (1) only considers nearest-neighbor interactions. We refer to a study on the string-string interaction strengths for the [111] direction in bcc iron [9]. The interaction between nearest-neighbor strings is estimated to be about two orders of magnitude larger than the interaction between second-nearest-neighbor strings,

which motivates our complete neglect of the second-nearest neighbors.

(ii) The MSFK string potential is linearized for strings that do not lie adjacent to the glide plane. This is consistent with linear elasticity theory.

(iii) The discrete Lagrangian (1) is brought to the continuum limit, replacing discrete differences in atomic displacement by first-order derivatives of a continuous displacement field; the displacement field is assumed to change slowly over the atomic spacing. This approximation is expected to become inaccurate for very narrow dislocation cores.

(iv) In the continuum limit the nonlinear string-string interaction is averaged over strings lying across the glide plane, giving rise to the effective string number  $\mathcal{Z}$ . This procedure neglects the relative staggering of atomic layers along the line direction, effectively treating the mismatch potential in a mean-field picture.

(v) The displacement field perpendicular to the Burgers vector is entirely neglected, consequently the far-field behavior of the displacement fields is inconsistent with the linear elasticity solution of the straight Volterra edge dislocation.

The approximations listed under the first four points most strongly influence the dislocation core region, leaving the far-field properties of the displacement fields unaffected. The neglect of the perpendicular displacement field however, see point (v), leads to an unphysical far-field behavior of the elastic fields; we are effectively assuming linear strain conditions instead of plane strain conditions.

### III. ANALYTICAL SOLUTION FOR THE FULL STRAIN FIELD OF AN EDGE DISLOCATION

It appears possible to extend the MSFK model into two dimensions by including the appropriate interactions between the atomic strings in the directions perpendicular to the Burgers vector. The detailed nature of such interactions is not of major interest as there is in principle an endless variety of interatomic potentials that all reproduce the elastostatic equations. We present one such example of a minimal two-dimensional discrete MSFK model in the appendix.

The two-dimensional MSFK model offers a physically motivated extension of the Peierls original description of the edge dislocation core, valid in the entire space and consistent with isotropic linear elasticity. The surface boundary value problem is unchanged by the presence of the transverse field  $u_y$ . We are hence justified in using a generalized elastostatic boundary value problem in two dimensions:

$$\begin{aligned} u_{x,xx}^+ + \frac{1-2\nu}{2(1-\nu)} u_{x,yy}^+ &= -\frac{1}{2(1-\nu)} u_{y,xy}^+, \quad y > 0 \\ u_{y,yy}^+ + \frac{1-2\nu}{2(1-\nu)} u_{y,xx}^+ &= -\frac{1}{2(1-\nu)} u_{x,yx}^+, \quad y > 0 \\ \lim_{y \rightarrow 0^+} \frac{4\pi}{p} u_{x,y}^+ &= \lim_{y \rightarrow 0^+} \sin\left(\frac{4\pi}{b} u_x^+\right). \end{aligned} \quad (19)$$

Following Peierls [3], the boundary value problem (19) can be solved by making an educated guess. We have found the following solution:

$$\begin{aligned}
 u_x &= \frac{b \operatorname{sgn}(y)}{2\pi} \left( \frac{\pi}{2} + \frac{1}{2(1-\nu)} \frac{\kappa^2 x|y|}{(\kappa x)^2 + (\kappa|y| + b)^2} - \arctan \left( \frac{\kappa x}{\kappa|y| + b} \right) \right) \\
 u_y &= \frac{b}{8\pi(1-\nu)} \left( \frac{2\kappa|y|(b + \kappa|y|)}{(\kappa x)^2 + (\kappa|y| + b)^2} - (1 - 2\nu) \ln \left( \frac{(\kappa x)^2 + (\kappa|y| + b)^2}{\kappa^2} \right) - 1 \right),
 \end{aligned}
 \tag{20}$$

where we define the rescaled constant  $\kappa$  to make the solution more readable:

$$\kappa \equiv \frac{2(1-\nu)}{3-2\nu} p.
 \tag{21}$$

Substituting the above equations into the boundary value problem (19) confirms the validity of this solution. The displacement field becomes identical to the known solution of the one-dimensional Peierls-Navarro model (15) at the glide plane in the limit  $y \rightarrow 0^+$ , see Eq. (16), though the crowdion width differs slightly. It is further evident that the solution reduces to the analytical form of the Volterra edge dislocation [2] in the  $p \rightarrow \infty$  limit:

$$\begin{aligned}
 \lim_{\kappa \rightarrow \infty} u_x &= u_x^{\text{Volterra}} = \frac{b}{2\pi} \left( \operatorname{sgn}(y) \frac{\pi}{2} + \frac{1}{2(1-\nu)} \frac{xy}{x^2 + y^2} - \arctan \left( \frac{x}{y} \right) \right) \\
 \lim_{\kappa \rightarrow \infty} u_y &= u_y^{\text{Volterra}} = \frac{b}{8\pi(1-\nu)} \left( \frac{y^2 - x^2}{x^2 + y^2} - (1 - 2\nu) \ln(x^2 + y^2) \right).
 \end{aligned}
 \tag{22}$$

#### IV. ANALYTICAL DERIVATION OF THE DISLOCATION CORE RADIUS

The general solution of the displacement field caused by a straight dislocation in an infinite elastic medium can be expressed in terms of cylindrical coordinates  $(\rho, \theta, z)$  as [10]:

$$\mathbf{u}(\rho, \theta) = v \ln(\rho) + \mathbf{u}_0(\theta) + \sum_{n=1}^{\infty} \mathbf{u}_n(\theta) \frac{1}{\rho^n},
 \tag{23}$$

where the first two terms represent the Volterra solution, and the Laurent series represents far-field corrections to the elastic field due to nonlinearities inherent to the dislocation core. The effect of the main contribution ( $n = 1$ ) to the elastic field has been thoroughly studied by Clouet *et al.* in isotropic and anisotropic elasticity [11–14], and was found to be of major importance for dislocation core energy calculations.

The effect of the dislocation core can be considered through the far-field corrections (23). However, this representation does not offer a definition of the transition radius between near and far field, commonly referred to as the dislocation core radius. In contrast, the analytical solution to the 2D-MSFK problem enables us to explicitly investigate the convergence behavior of the Laurent series.

For simplicity we shall only consider the solution on the upper half plane, that is for  $y > 0$  or  $\theta \in (0, \pi)$ . The series expansion of the 2D-MSFK displacement fields (20) is taken for  $\rho \rightarrow \infty$  [15]:

$$\begin{aligned}
 u_x(\rho, \theta) &= u_x^{\text{Volterra}}(\rho, \theta) + \sum_{n=1}^{\infty} \frac{u_{x,n}(\theta)}{\rho^n} \\
 u_y(\rho, \theta) &= u_y^{\text{Volterra}}(\rho, \theta) + \sum_{n=1}^{\infty} \frac{u_{y,n}(\theta)}{\rho^n},
 \end{aligned}
 \tag{24}$$

with the coefficients found as:

$$\begin{aligned}
 u_{x,n}(\theta) &= (-1)^n \frac{b}{2\pi} \left( \frac{b(3-2\nu)}{2p(1-\nu)} \right)^n \\
 &\quad \times \left( \frac{\sin(\theta) \cos \left( \frac{n\pi}{2} - n\theta - \theta \right)}{2(1-\nu)} \right. \\
 &\quad \left. - \frac{1}{n} \sin \left( \frac{n\pi}{2} - n\theta \right) \right) \\
 u_{y,n}(\theta) &= \frac{b}{4\pi(1-\nu)} \left( \frac{b(3-2\nu)}{2p(1-\nu)} \right)^n \\
 &\quad \times \left( \sin(\theta) \sin \left( \frac{n\pi}{2} + n\theta + \theta \right) \right. \\
 &\quad \left. + \frac{1-2\nu}{n} \cos \left( \frac{n\pi}{2} + n\theta \right) \right).
 \end{aligned}
 \tag{25}$$

Note that the term not included in the Laurent series is the known Volterra displacement field (22). Using the Cauchy-Hadamard formula for the radius of convergence of the power series

$$\rho_C^{-1} = \limsup_{n \rightarrow \infty} |u_{\alpha,n}|^{\frac{1}{n}},
 \tag{26}$$

we find the radii of convergence  $\rho_C$  of the  $u_x(\rho, \theta)$  and  $u_y(\rho, \theta)$  power series to be identical:

$$\rho_C = \frac{b}{p} \left( \frac{3-2\nu}{2(1-\nu)} \right).
 \tag{27}$$

In conclusion, the linear-elasticity representation of the elastic fields (23) diverges for distances smaller than  $\rho_C$ . For smaller radii  $\rho < \rho_C$  the nonlinearity of the glide-plane boundary value problem becomes dominant, and the analytical solution cannot be represented in terms of the linear elasticity far-field solution anymore. For all intents and purposes, the radius of convergence  $\rho_C$  can be interpreted as the dislocation core

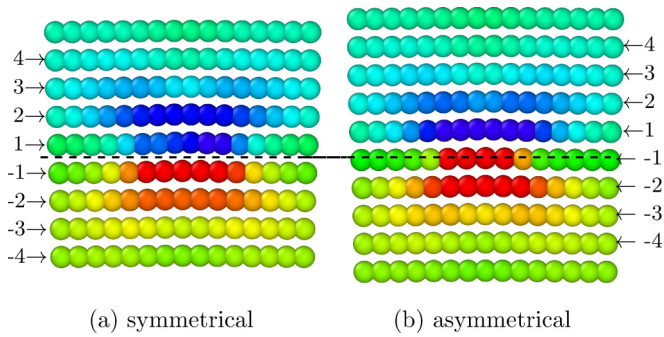


FIG. 3. Atomistic strain fields  $u_{x,x}$  for the tungsten  $\frac{1}{2}[111](10\bar{1})$  edge dislocation core. Two repeating configurations are found along the  $[\bar{1}21]$  line direction: a symmetric (a) and an asymmetric (b). Blue color corresponds to the compressive strain and red color to the tensile strain. The first few atomic rows above and below the glide-plane (black, dashed line) are indexed as shown in the figure.

radius. It is of further interest to note that the radius of convergence is independent of the angle  $\theta$ , the dislocation core is hence indeed bound by a cylinder with radius  $\rho_C$  surrounding the dislocation line, as commonly pictured.

## V. ATOMISTIC SETUP

We now benchmark the model with the reference data derived from atomistic simulations. Atomistic simulations were performed using LAMMPS [16] for iron and tungsten, for two different interatomic potentials for each material. The simulation cell was initialized as a pristine bcc lattice with the coordinate system aligned along  $x = [111]$ ,  $z = [\bar{1}21]$ , and  $y = [\bar{1}01]$ . The crystal lattice fills a volume of  $120 \times 120 \times 6$  lattice units with periodic boundary conditions applied in the line direction  $z = [\bar{1}21]$ . A dislocation was introduced by applying anisotropic linear-elastic displacement field of the  $\frac{1}{2}[111](10\bar{1})$  edge dislocation at the box center, using elastic constants appropriate for the chosen interatomic potential. Atomic coordinates were relaxed while keeping atoms beyond a distance of 100 lattice units from the dislocation line fixed at positions corresponding to a solution in an infinite elastic medium. Atomistic strain and displacement fields were computed in reference to the perfect bcc structure.

Two alternating atomic configurations are found along the  $[\bar{1}21]$  line direction, see Fig. 3. The  $u_{x,x}$  strain field in one of the configurations is strongly asymmetric at the core, as the apparent height of the glide plane is not centered between the atomic rows. Our comparison of atomistic and continuum strain fields is therefore solely focused on the symmetric configuration.

The surface structure constant  $p$  for each case is found by fitting the  $u_{x,x}$  component of the continuum strain field to the atomistic strain fields at the position of two atomic rows above and below the glide plane. We refer to Table I for a comparison of the fitted constants to their MSFK value as determined by the crystal structure (21). The fitted values for  $p$  are found to vary little between the various potentials. The value of the constant does not depend on the details of the interatomic potentials, though that is only true within the approximations inherent to MSFK. It is therefore not surprising that atomistic simulations

TABLE I. Surface-structure constant  $p$  as fitted for tungsten and iron and as computed from MSFK (21). The dislocation width  $w(p)$  is computed in the glide plane according to the MSFK model.

Material	Model	$p$	$w(p)/b$
W	Marinica <i>et al.</i> [17]	1.37	2.48
	Mason <i>et al.</i> [18]	1.70	2.00
Fe	Ackland <i>et al.</i> [19]	1.41	2.41
	Gordon <i>et al.</i> [20]	1.66	2.04
	MSFK <sup>a</sup>	1.89	1.79

<sup>a</sup>For  $\nu = 0.28$  and  $G^s = 3/2$  (see Fig. 2),

show small variation of the surface structure constant even for the same dislocation geometry.

A comparison of the continuum and atomistic strain fields for tungsten computed using the Marinica *et al.* [17] EAM4 potential is shown in Fig. 4. The MSFK and atomistic strain fields for tungsten are in good agreement everywhere in space. The strain fields for iron, see the Supplemental Material [21], deviate slightly at larger distances from the core. Iron exhibits considerable elastic anisotropy and therefore requires an anisotropic linear elasticity model.

The magnitude of the atomistic tensile strain is generally higher than the atomistic compressive strain. Several phenomena can affect the symmetry of the strain fields. For instance, the glide plane may not be evenly centered between the atomic rows, which is the case for configuration (b) in Fig. 3. Another explanation is that in many empirical potentials it takes more energy to compress atomic bonds than to stretch them, hence tensile strains will be larger than compressive strains under equal stress.

We have also repeated the same procedure for the  $[100](010)$  edge dislocation that has a comparatively narrow core width. This is reflected in the MSFK surface structure constant  $p$  acquiring the value of 8.0. The MSFK model is unable to match the atomistic strain fields, as these are more localized than what is permitted by the Volterra solution in the limit  $p \rightarrow \infty$ . The atomistic strain fields for the  $[100](010)$  configuration vary strongly on the scale of interatomic lattice spacing, hence it can be reasoned that the continuum approximation inherent to the MSFK model becomes invalid.

## VI. PEIERLS MIGRATION BARRIER

There is no energy barrier associated with dislocation glide in the continuum model, as the displacement fields are translationally invariant in the direction of the Burgers vector. In an atomic lattice however, the displacement fields are resolved discretely on lattice sites, consequently the total elastic energy per dislocation length  $L$  varies periodically as a function of the displacement field center  $(x_0, y_0)$ . The exact analytical solution of the displacement fields in the 2D-MSFK model enables us to estimate the barrier with little computational effort.

The dislocation glide is considered to proceed along the minimum energy pathway, defined as the trajectory connecting the global energy minima corresponding to the adjacent periodic cells with the smallest possible energy barrier. This energy barrier is commonly referred to as the Peierls migration barrier [3]. We compute the barrier by evaluating the discrete

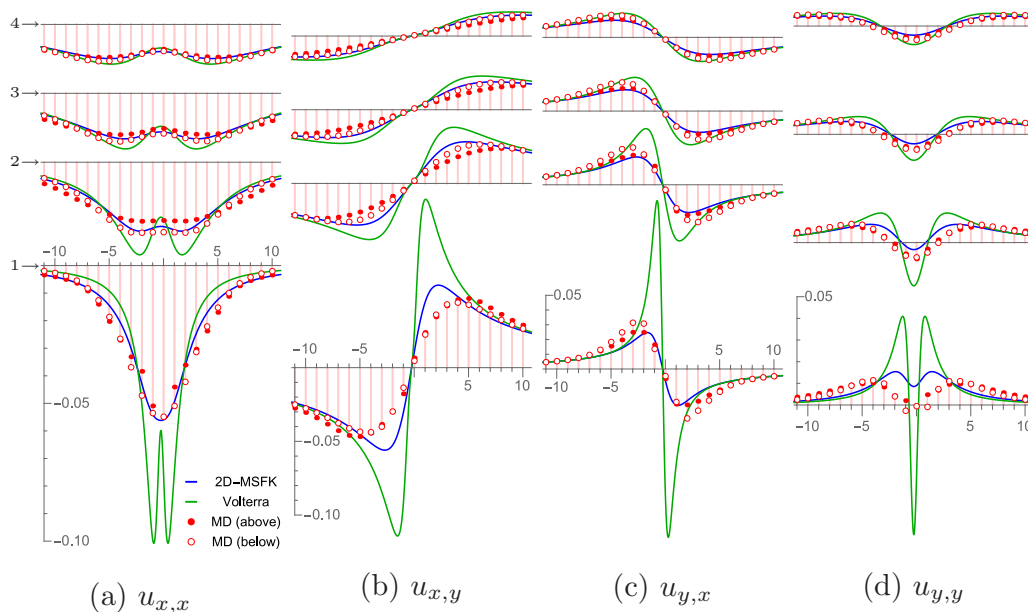


FIG. 4. Strain fields in the vicinity of  $\frac{1}{2}[111](10\bar{1})$  edge dislocation core in tungsten. The strain fields at the first four atomic rows above (compressive strain, filled dots) and below (tensile strain, unfilled dots) the glide plane are pictured here, according to the indices in Fig. 3. The  $x$  axis is given in units of the Burgers vector length  $b$ , and the  $y$  axis refers to the dimensionless strains  $u_{i,j}$ . Figures (a), (b), (c), and (d) refer to strains  $u_{x,x}$ ,  $u_{x,y}$ ,  $u_{y,x}$ , and  $u_{y,y}$ , respectively. Graphs for the same strain use identical axes scales, and the tensile strains pictured here are point reflected.

expressions for the dislocation energy using the continuum solution [22] for the displacement fields  $u_x$  and  $u_y$  as shown in Eq. (22).

The migration pathway is approximated to lie along the fixed height  $y_0 = y_{\min}$  where the energy minimum ( $x_{\min}$ ,  $y_{\min}$ ) of the bulk energy  $\mathcal{L}_{\text{bulk}}(x_0, y_0)$  occurs [23]. The Peierls barrier is then given by:

$$\mathcal{L}_{\text{net}}(x_0, y_0) = \mathcal{L}_{\text{bulk}}(x_0, y_0) + \mathcal{L}_{\partial\Omega}(x_0, y_0) \quad (28a)$$

$$V_P = (\max_{x_0 \in [0, b]} \mathcal{L}_{\text{net}}(x_0, y_{\min}) - \min_{x_0 \in [0, b]} \mathcal{L}_{\text{net}}(x_0, y_{\min})) / L. \quad (28b)$$

We express the shear modulus  $\mu$  in terms of the MSFK force constants by comparing the MSFK equation of motion with the elastostatic equation (before canceling constants):

$$\mu = m\omega^2 l^2 \eta G. \quad (29)$$

Let  $x_{n,j}$ ,  $y_{n,j}$ , and  $z_{n,j}$  be the coordinates of the pristine, unstrained lattice. The interfacial energy (4b) is expressed as:

$$\begin{aligned} \mathcal{L}_{\partial\Omega}(x_0, y_0) = & -\frac{\mu b^2}{\pi^2 l^2 \eta G} \sum_{\substack{j \in \Omega^+ \\ j+h \in \Omega^-}} \\ & \times \sum_{n=-\infty}^{\infty} \sin^2 \left( \frac{\pi}{b} ((u_x)_{n,j} - (u_x)_{n,j+h}) \right), \end{aligned} \quad (30)$$

where  $(u_i)_{n,j} = u_i(x_{n,j} - x_0, y_{n,j} - y_0)$  represents the displacement field in  $i$  direction according to the continuum solution (22), offset by the dislocation center  $(x_0, y_0)$ . The bulk energy is expressed in terms of the standard isotropic

elastic energy evaluated at the discrete lattice coordinates:

$$\mathcal{L}_{\text{bulk}}(x_0, y_0) = -\frac{1}{2\eta} \sum_{j \in \mathbb{R}^3} \sum_{n=-\infty}^{\infty} \sum_{ipkl} c_{ipkl} (\varepsilon_{ip})_{n,j} (\varepsilon_{kl})_{n,j}, \quad (31)$$

where  $c_{ipkl}$  is the isotropic stiffness tensor,  $\eta$  is the atom number density, and  $(\varepsilon_{ip})_{n,j}$  is the strain tensor:

$$(\varepsilon_{ip})_{n,j} = \frac{1}{2} ((u_{i,p})_{n,j} + (u_{p,i})_{n,j}). \quad (32)$$

The total energy (28b) is evaluated numerically for edge dislocations in tungsten, using the structure constants appropriate to the  $\frac{1}{2}[111](10\bar{1})$  and  $[100](010)$  orientations, as shown in Table II. The Peierls barrier in the atomistic reference is obtained by migrating one dislocation in a dipole pair using the nudged elastic band method [24], subsequently correcting the energy for elastic interactions. The  $\frac{1}{2}[111](10\bar{1})$  and  $[100](010)$  dislocations have a migration period of  $b/3$  and  $b$ , respectively.

The MSFK and MD barriers for the  $[100](010)$  dislocation are found to be similar. The  $\frac{1}{2}[111](10\bar{1})$  barrier is considerably lower in MD, however in the MSFK model it vanishes almost entirely due to a combination of a wide dislocation core and staggered atomic stacking in the  $[1\bar{2}1]$  line direction. We con-

TABLE II. Peierls barrier  $V_P$  for the tungsten  $\frac{1}{2}[111](10\bar{1})$  and  $[100](010)$  edge dislocations computed using appropriate parameters for tungsten ( $\mu = 160$  GPa,  $\nu = 0.28$ ).

Type	$p$	$V_P^{\text{MSFK}}/\text{meV}\text{\AA}^{-1}$	$V_P^{\text{MD}}/\text{meV}\text{\AA}^{-1}$
$\frac{1}{2}[111](10\bar{1})$	1.89	$<10^{-4}$	0.918
$[100](010)$	8.00	143	274

sidered the continuum displacement fields as identical for every atomic layer in the  $[1\bar{2}1]$  direction, effectively neglecting core interactions between atomic layers. More sophisticated models based on the Peierls-Nabarro solution can attain migration barriers quantitatively comparable to those found in atomistic simulations [25–27].

## VII. CONCLUSION

In this treatise, we have systematically derived and validated a continuum nonsingular model that predicts strain fields of an edge dislocation, including its core. Predictions derived from the model are consistent with atomistic simulations performed using several interatomic potentials, for the  $\frac{1}{2}[111](10\bar{1})$  edge dislocation in iron and tungsten. Analytical solutions found for the edge dislocation strain fields are explicit and exact.

The model provides a physically motivated connection between equations of linear elasticity and the Peierls-Nabarro boundary value problem. Although the model is in principle parameter free, the surface structure constant  $p$  offers a convenient way of controlling the dislocation core width. For wider dislocation cores the constant  $p$  can be fitted to reproduce atomistic strain fields, while for narrow dislocation cores some alternative measures, such as line-tension, need to be considered due to the limitations inherent to the continuum approximation.

Further work can be well motivated by applying the model to more complex systems, such as screw and mixed dislocations, interacting dislocation segments, and most importantly line tension calculations for curved dislocation. The treatment of mixed or curved dislocations motivates an extension of the MSFK model to three dimensions. The availability of reference data from atomistic simulations offers a promising testing ground for these applications.

## ACKNOWLEDGMENTS

This work has been carried out within the framework of the EUROfusion Consortium and has received funding from the Euratom research and training programme 2014-2018 under Grant Agreements No. 633053 and No. 755039. Also, it has been partially funded by the RCUK Energy Programme (Grant No. EP/P012450/1). The views and opinions expressed herein do not necessarily reflect those of the European Commission. Useful conversations with Jacob B.J. Chapman and Andrew J. London are gratefully acknowledged.

## APPENDIX: THE TWO-DIMENSIONAL MULTISTRING FRENKEL-KONTOROVA MODEL

In the one-dimensional MSFK model we consider atoms to interact harmonically with their nearest neighbors in the direction of the Burgers vector. The first step is to also consider atoms to interact harmonically with their nearest neighbors in the perpendicular direction, with neighboring strings interacting through a sinusoidal potential. If we let  $\mathbf{b} \parallel \hat{e}_x$  and  $\mathbf{b} \perp \hat{e}_y$ , assuming plane-strain conditions in the  $z$  direction, we obtain an additional equation of motion for the

transversal field  $u_y$ :

$$u_{y,yy} + \frac{\omega^2 l^2 G}{c^2} u_{y,xx} = 0. \quad (\text{A1})$$

We have chosen the stiffness and string-interaction strength such that identical prefactors as for the  $u_x$  field are obtained, as required to attain isotropic elasticity. We do not need to split the transversal field between the upper and lower domains  $\Omega^\pm$  because edge dislocation discontinuity only applies to the boundary conditions of  $u_x$ . A comparison with the elastostatic equations (12) makes clear that we need to further add coupling between fields  $u_x$  and  $u_y$ .

For the sake of simplicity, we shall restrict following discussion to atoms arranged in a two-dimensional square lattice with a spacing of  $b$ . The displacement fields of an atom originally placed at  $\mathbf{r}_{n,m} = nb\hat{e}_x + mb\hat{e}_y$  are written as  $u_{n,m}^x$  and  $u_{n,m}^y$ . We add a cross coupling term to the discrete Lagrangian:

$$\begin{aligned} \mathcal{L}_{xy} = & \sum_{\substack{n,m \\ n' = \pm 1 \\ m' = \pm 1}} n' m' V_0 \sin\left(\frac{\pi}{b}(u_{n+n',m+m'}^x - u_{n,m}^x)\right) \\ & \times \sin\left(\frac{\pi}{b}(u_{n+n',m+m'}^y - u_{n,m}^y)\right). \end{aligned} \quad (\text{A2})$$

Approximating the displacement differences to first order according to

$$u_{n\pm 1, m\pm 1}^i = u_{n,m}^i \pm b \frac{\partial u_{n,m}^i}{\partial n} \pm b \frac{\partial u_{n,m}^i}{\partial m}, \quad (\text{A3})$$

the Lagrangian is linearized in the continuum limit:

$$L_{xy} = \eta \int dV 4\pi^2 V_0 (u_{x,x} u_{y,y} + u_{x,y} u_{y,x}). \quad (\text{A4})$$

Using the principle of least action we see that the coupling Lagrangian contributes mixed terms to the equations of motion:

$$\begin{aligned} u_{x,xx}^\pm + \frac{\omega^2 l^2 G}{c^2} u_{x,yy}^\pm + 4\pi^2 V_0 u_{y,xy} &= 0 \\ u_{y,yy} + \frac{\omega^2 l^2 G}{c^2} u_{y,xx} + 4\pi^2 V_0 u_{x,xy}^\pm &= 0. \end{aligned} \quad (\text{A5})$$

We are free to choose the coupling-potential strength  $V_0$  such that the correct form for linear elasticity is obtained:

$$4\pi^2 V_0 = \frac{1}{2(1-\nu)} = \frac{\omega^2 l^2 G}{c^2} - 1, \quad (\text{A6})$$

where the MSFK definition of Poisson's ratio (14) was used. This leads to the elastostatic equations:

$$\begin{aligned} u_{x,xx}^\pm + \frac{1-2\nu}{2(1-\nu)} u_{x,yy}^\pm &= -\frac{1}{2(1-\nu)} u_{y,xy} \\ u_{y,yy} + \frac{1-2\nu}{2(1-\nu)} u_{y,xx} &= -\frac{1}{2(1-\nu)} u_{x,xy}^\pm. \end{aligned} \quad (\text{A7})$$

In summary, we have derived the elastostatic equations from a two-dimensional discrete multistring Frenkel-Kontorova model for a simple cubic crystal structure.

It remains to characterize the influence of the cross-coupling Lagrangian on the boundary value problem. Similarly to the

1D-MSFK case, we consider strings lying on opposing sides of the dividing surface:

$$\begin{aligned} \mathcal{L}_{xy,\partial\Omega} = & -2 \sum_{\substack{n,m \\ n'=\pm 1}} n' V_0 \sin\left(\frac{\pi}{b}(u_{n+n',m-1}^x - u_{n,m}^x)\right) \\ & \times \sin\left(\frac{\pi}{b}(u_{n+n',m-1}^y - u_{n,m}^y)\right). \end{aligned} \quad (\text{A8})$$

Exploiting the symmetries of the straight edge dislocation displacement fields as known from the linear elasticity solution,

we arrive at the interfacial Lagrangian in the continuum limit:

$$\mathcal{L}_{xy,\partial\Omega} = \frac{4V_0}{b^2} \int_{\partial\Omega} dS \cos(\pi u_{x,x}^-) \sin\left(\frac{2\pi}{b} u_x^+\right) \sin(\pi u_{y,x}). \quad (\text{A9})$$

The interfacial Lagrangian vanishes because  $u_{y,x}$  is an odd function with respect to  $x$ . For generally curved dislocations that is not the case; neglecting the effect of transverse fields on the boundary value problem is equivalent to the planar core approximation commonly used in Peierls-Nabarro models. The derivation for a more general crystal lattice follows equivalently, but the notation is opaque as we would be handling two separate sets of string vectors, displacement vectors, and string distances.

- 
- [1] B. A. Szajewski, F. Pavia, and W. A. Curtin, *Modell. Simul. Mater. Sci. Eng.* **23**, 085008 (2015).
- [2] P. M. Anderson, J. P. Hirth, and J. Lothe, *Theory of Dislocations* (Cambridge University Press, Cambridge, 2017).
- [3] R. Peierls, *Proc. Phys. Soc.* **52**, 34 (1940).
- [4] V. V. Bulatov and W. Cai, *Computer Simulations of Dislocations* (Oxford University Press, Oxford, 2006), Vol. 3, Chap. 8.
- [5] G. Lu, in *Handbook of Materials Modeling* (Springer, Dordrecht, 2005), pp. 793–811.
- [6] G. Schoeck, *Mater. Sci. Eng. A* **400**, 7 (2005).
- [7] F. R. N. Nabarro, *Proc. Phys. Soc.* **59**, 256 (1947).
- [8] S. L. Dudarev, *Philos. Mag.* **83**, 3577 (2003).
- [9] M. R. Gilbert and S. L. Dudarev, *Philos. Mag.* **90**, 1035 (2010).
- [10] J. D. Eshelby, W. T. Read, and W. Shockley, *Acta Metall.* **1**, 251 (1953).
- [11] E. Clouet, L. Ventelon, and F. Willaime, *Phys. Rev. Lett.* **102**, 055502 (2009).
- [12] E. Clouet, *Philos. Mag.* **89**, 1565 (2009).
- [13] E. Clouet, *Phys. Rev. B* **84**, 224111 (2011).
- [14] E. Clouet, L. Ventelon, and F. Willaime, *Phys. Rev. B* **84**, 224107 (2011).
- [15] The series expansion of the logarithmic term in  $u_y$  is taken by splitting it up:  $\ln(a + bR + cR^2) = \ln(aR^{-2} + bR^{-1} + c) + \ln(R^2)$ . Only the first term is expanded, while the second term enters the standard Volterra solution.
- [16] S. Plimpton, *J. Comput. Phys.* **117**, 1 (1995).
- [17] M.-C. Marinica, L. Ventelon, M. R. Gilbert, L. Proville, S. L. Dudarev, J. Marian, G. Bencteux, and F. Willaime, *J. Phys.: Condens. Matter* **25**, 395502 (2013).
- [18] D. R. Mason, D. Nguyen-Manh, and C. Becquart, *J. Phys.: Condens. Matter* **29**, 505501 (2017).
- [19] G. J. Ackland, D. J. Bacon, A. F. Calder, and T. Harry, *Philos. Mag. A* **75**, 713 (1997).
- [20] P. A. Gordon, T. Neeraj, and M. I. Mendelev, *Philos. Mag.* **91**, 3931 (2011).
- [21] See Supplemental Material at <http://link.aps.org/supplemental/10.1103/PhysRevMaterials.2.083803> for strain fields of the bcc tungsten and iron edge dislocation for various interatomic potentials.
- [22] The continuum solution can be used for a discrete lattice if the displacement fields vary slowly in comparison to the atomic spacings. Hence we expect greater uncertainties for the [100](010) configuration.
- [23] The bulk energy  $\mathcal{L}_{\text{bulk}}$  diverges with respect to system size, while the interfacial energy  $\mathcal{L}_{\partial\Omega}$  remains finite. The change in bulk energy for dislocation translation however is finite. Consequently, the energy barrier is a well-defined finite quantity and the migration pathway passes through energy minima of the bulk energy.
- [24] G. Henkelman, B. P. Uberuaga, and H. Jónsson, *J. Chem. Phys.* **113**, 9901 (2000).
- [25] H. Wei, Y. Xiang, and P. Ming, *Commun. Comput. Phys.* **4**, 275 (2008).
- [26] K. Kang, V. V. Bulatov, and W. Cai, *Proc. Natl. Acad. Sci. U.S.A.* **109**, 15174 (2012).
- [27] G. Liu, X. Cheng, J. Wang, K. Chen, and Y. Shen, *Sci. Rep.* **7**, 43785 (2017).